EXPERIMENTAL EVIDENCE FOR LIQUID IRON ALLOY FLOTATION ON SILICATE MELT N.J. Hooper[1], N. Dygert[1], R. Hrubiak[2], B.D. Monteleone[3], and B.A. Anzures[1,4,5]. [1]Earth and Planetary Sciences, University of Tennessee, (nhooper3@vols.utk.edu; ndygert1@utk.edu); [2]High Pressure Collaborative Access Team, Argonne National Laboratory; [3]Northeast National Ion Microprobe Facility, Woods Hole Oceanographic Institution; [4]Lunar and Planetary Institute/USRA; [5]ARES, NASA Johnson Space Center.

Introduction: We report the results of experiments conducted in a VX-3 Paris-Edinburgh apparatus at Beamline 16-BM-B, Argonne National Laboratory, that produced liquid metal flotation on a silicate liquid (e.g., Fig. 1). This behavior was observed in experiments conducted at 0.1-1 GPa and 1425-1885°C over two experimental sessions. We report our methods and observations, discuss initial results of characterization of the run products, and present a preliminary analysis.

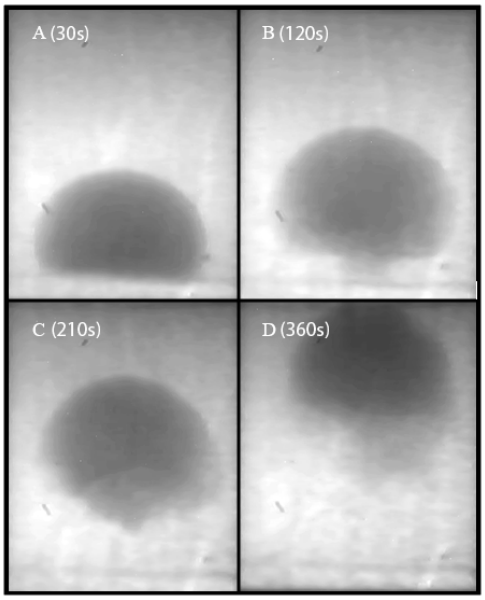

Fig. 1: X-ray radiograph sequence illustrating the flotation of the liquid metal (darker material) in silicate liquid at t=30, 120, 210, 360s (a)-(d).

Starting Materials: The starting composition used in these experiments is a titanian ferrobasalt representing a late-stage lunar magma ocean liquid (FR-1290 [1]). Experimental powder was prepared from reagent grade oxide and carbonate powders. After 5h grinding in ethanol in an agate mortar, the powder was decarbonated in an alumina crucible at 800°C in air for 4 hours. A portion of the decarbonated powder was separated and fused in a H-CO_2 gas mixing furnace at an fO_2 ≲5 log units below the iron-wüstite buffer, quenched in air, then reground into a powder in ethanol. The bulk composition was determined from electron microprobe analysis of the unconditioned portion of starting material (fused in a piston cylinder apparatus) and is reported in Table 1, along with representative experimental run product compositions.

Experimental methods: Experiments were conducted in a large volume Paris-Edinburgh press. The experimental assembly consists of a graphite inner capsule within a boron nitride (BN) sleeve and a graphite resistance heater, sandwiched between two cone shaped anvils (Fig. 2). The assembly is designed for falling sphere viscometry experiments; a dense rhenium sphere is placed within the starting material powder near the top of cylinder. The powder is brought to a near-liquidus temperature and then ramped to a superliquidus condition, producing flash melting. Polychromatic X-rays from the synchrotron pass through the assembly and are attenuated by high Z materials in capsule (normally the rhenium sphere). In typical experiments, a high-speed radiography system behind the apparatus images the fall of the rhenium sphere, and the viscosity of the silicate liquid is calculated from its terminal velocity [e.g., 2]. The behavior of the highly reduced starting material investigated in the present study was quite different.

Table 1. Compositions of starting materials and run products determined by electron microprobe at the University of Tennessee. †Reported in wt%. *Reported in normalized atomic %.

	Starting† material	**Silicate† liquid**		**Iron* Alloy**
SiO_2	43.7	48.5	Fe	63.9
TiO_2	3.8	4.7	Re	2.3
Al_2O_3	9.5	14.5	B	0.6
CaO	11.8	12.3	C	33.2
FeO	28.2	13.5	Total	100
MgO	0.3	1.2		
MnO	0.6	0.7		
Na_2O	0.7	0.9		
K_2O	0.2	0.3		
Total	98.8	97.1		

Observations: In the current experiments, iron metal alloy (darker region, Fig. 1) initially dispersed throughout the experimental charge, coalesces into a sphere near the center of the capsule, then stalls or sinks toward the capsule floor before buoyantly rising toward the graphite roof. Experiments were run with and without rhenium spheres and the iron flotation behavior was consistent between them. When rhenium spheres are present they are quickly dissolved upon contact with the metal alloy (e.g., Table 1). Fig. 1 displays X-ray radiograph images of an experiment conducted at 1 GPa and 1425°C. Of 10 experiments analyzed, five were observed to exhibit flotation behavior similar to that shown in Fig. 1. In experiments exhibiting non-buoyant behavior, the liquid metal alloy flattens into an oblate spheroid on the capsule floor or wall, presumably adhering by surface tension. In some cases, it then creeps up the graphite wall.

Analysis: We considered the possibility that convection in the experimental cell pushed the liquid metal droplets upward. Because the hotspot in the assembly is near the jacket wall mid-way from the top, convection would push metal droplets downward toward the assembly floor (Fig. 2), inconsistent with the observations.

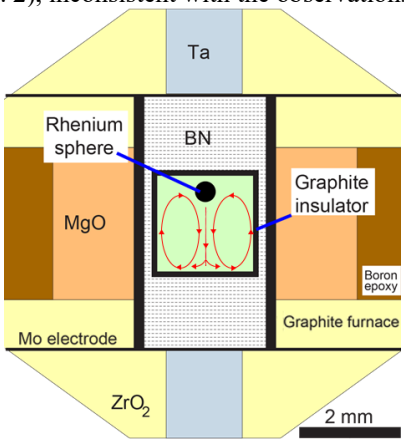

Figure 2: Schematic of the assembly design (Figure modified from [2]) depicting anticipated convection behavior in the experimental cell (red flow paths).

Degassing of volatiles from the starting composition may cause bubble nucleation and accumulation on the metal-silicate melt interface. This would lead to metal flotation if the effective density of the metal sufficiently decreased to make it buoyant. An analogous process has been proposed (and experimentally demonstrated) to explain the accumulation of dense Fe-oxide crystals along magma chamber roofs [3]. In those experiments, magnetite flotation occurred as fluid bubbles nucleated on oxide surfaces during decompression. We note that bubble formation in our experiments is supported by sectioned experimental run products which exhibit numerous bubbles in the metal and silicate liquid. Bubbles are not obvious in the X-ray radiographs at the metal-silicate interface, but the radiographs are not clear enough to establish whether they are present during the experimental runs.

Calculated densities of liquid iron, liquid iron-C alloy, and the coexisting silicate liquid are shown in Fig. 3 as a function of pressure. Pressure-density estimates were computed using a third-order Birch-Murnaghan equation of state (EOS). Assuming the floating metal is represented by an Fe-C alloy (Table 1), the alloy droplet is more than twice as dense as the coexisting silicate liquid (Fig. 3) [4-7]. Using these density data, we calculate the required bubble fraction for neutral buoyancy:

$$\rho_{silicate} = \rho_{metal} \times (1-\varphi_{bubbles}) + \rho_{bubbles} \times \varphi_{bubbles} \quad (1).$$

Making the simplifying assumption that the bubble density is 0, the bubble fraction must be ~50% (at atmospheric pressure).

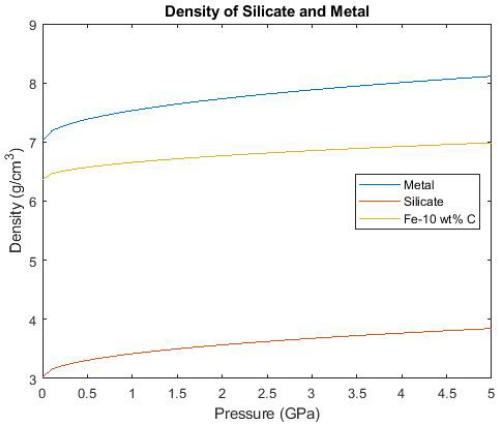

Figure 3: Profile of density for silicate, liquid metal, and liquid Fe-10 wt% C alloy computed from a Birch-Murnaghan EOS. The calculations imply a density difference of ~3.5 g/cm^3 between the metal and silicate.

Partitioning of light elements other than C into the metal alloy would further reduce its density. Quenched experimental run products were analyzed by Secondary Ion Mass Spectrometry (SIMS) at Woods Hole Oceanographic Institution. An analytical routine was developed to measure O, H, N, B, and C in the metals and glasses, using NIST steel reference materials and silicate glass reference materials. The data are currently being interpreted, but demonstrate measurable concentrations of volatiles other than C in the experiments.

Implications: Asteroid 16 Psyche has radar reflectance and optical properties suggesting an iron and/or iron-silicate crust, but a bulk density of 3400-4100 kg/m^3, consistent with a porous and/or silicate-rich interior [8,9]. Ferrovolcanism models have been proposed to explain this structure [10,11], where downward crystallization of a liquid iron core produces vertical migration of pressurized light element-rich liquid Fe alloy, perhaps into an overlying silicate mantle. If conditions analogous to our experiments can exist in planetesimals with magma oceans, metal flotation on silicate liquid may provide an alternative explanation for producing metal-rich regions at shallow depths within asteroids with rocky interiors.

References: [1] Longhi, J., 2003, JGR, 108, 5083. [2] Kono, Y., et al., 2014, PEPI, 228, 269-280. [3] Knipping, J.L., et al., 2019, Sci. Rep. 9, 3852. [4] Dorogokupets, P., et al., 2017, Sci. Rep. 7, 41863. [5] Bajgain, S.K., et al., 2021, Commun. Earth Environ. 2, 165. [6] Jimbo, I., et al., 1993, Metall. Mater. Trans. B 24, 5-10. [7] Jing, Z. & Karato, S., 2008, EPSL 272, 1-2. [8] Elkins-Tanton, L.T., et al., 2020, JGR Planets 125. E2019JE006296. [9] Shepard, M.K., et al., 2021, Planet. Sci. J. 2, 125. [10] Abrahams, J.N.H. & Nimmo, F., 2019, GRL 46, 5055-5064. [11] Johnson, B.C., et al., 2020. Nat. Astron. 4, 41-44.